

Reactions induced by 30 MeV ^3He beam on ^9Be : Cluster transfer reactions

Urazbekov B A^{1,2,3}, Issatayev T^{1,2,4*}, Lukyanov S M⁴,
Azhibekov A^{2,4,5}, Denikin A S^{4,6}, Mendibayev K^{2,4},
Janseitov D M^{2,3,7}, Penionzhkevich Yu E⁴, Kuterbekov K A¹,
Zholdybayev T K^{2,7}

¹Gumiliyev Eurasian National University, 2 Satpayev Str, Astana, Kazakhstan

²Institute of Nuclear Physics, 1 Ibragimov Str, Almaty, Kazakhstan

³Bogolubov Laboratory of Theoretical Physics, JINR, 20 Joliot Curie Str, Dubna, Russia

⁴Flerov Laboratory of Nuclear Reactions, JINR, 20 Joliot Curie Str, Dubna, Russia

⁵Korkyt-ata State University, 29A Aiteke-Byi Str, Kyzylorda, Kazakhstan

⁶Dubna State University, 19 Universitetskaya Str, Dubna, Russia

⁷Al-Farabi Kazakh National University, Almaty, Kazakhstan

E-mail: *issatayev@jinr.ru

Abstract. An experiment has been carried out for studying the cluster structure of ^9Be induced by the ^3He ions at the energy of 30 MeV. As results of the nuclear reaction $^3\text{He} + ^9\text{Be}$ the differential cross sections for the exit channels – elastic, inelastic, $\alpha + ^8\text{Be}$, $^6\text{He} + ^6\text{Be}$, $^6\text{Li} + ^6\text{Li}$, and $^7\text{Be} + ^5\text{He}$ – were measured.

Elastic and inelastic scattering data are treated within both the optical model and Coupled channels method. A new set of optical potential was taken for the elastic scattering. The deformation parameter δ_2 was established for the transition $3/2 \rightarrow 5/2$.

Cluster transfer reactions are analyzed by means of the coupled reaction channels method. The nuclear reactions with the exit channels $^6\text{He} + ^6\text{Be}$, $^6\text{Li} + ^6\text{Li}$, and $^7\text{Be} + ^5\text{He}$ are complemented by two-step transfer mechanisms. The contribution of each reaction mechanisms are shown, and compared with the findings of other authors.

Keywords: cluster transfer, reaction mechanisms, coupled equations

Introduction

In light nuclei, e.g. with $A < 12$, in most cases the nucleons may form a group. The group in nuclear physics is often called the cluster. Their relative motion determines general characteristics and properties. In this manner, studying the cluster structure of the light nuclei has become one of the prior tasks of nuclear physics with regard to the theory and experimental explorations.

The nucleus ^9Be is an attractive nucleus due to its many internal properties. Low binding energy of the p -shell neutron -1.66 MeV (e.g., see [1]), large quadrupole moment $+53.3 \pm 3$ mb [2, 3], and positive parity in the first excited state $\frac{1}{2}^+$ at 1.684 MeV (e.g., see [1]) – all of these experimental data points out its unique structure. Therefore, in the cluster model framework the nucleus can be supposed to have the configurations, such as $2\alpha + n$, $\alpha + ^5\text{He}$, $^8\text{Be} + n$, and other.

The cluster structure of ^9Be has been extensively studied within the various approaches [4–9]. In recent studies from Refs. [10, 11], the elastic scattering data of α -particles and of d on ^9Be have been treated within the cluster models $\alpha + ^5\text{He}$, and $^8\text{Be} + n$. Authors showed that on the example of the elastic scattering, the interaction potentials of projectiles can be treated by means of the cluster folding model within the configurations $\alpha + ^5\text{He}$ and $^8\text{Be} + n$. Moreover, at the backward angles the spectroscopic amplitudes were extracted in the calculations of the elastic transfer reactions.

It is interesting to note an analysis of the two-neutron transfer in the nuclear reactions induced by ^7Be radioactive beam on the target nucleus ^9Be [12]. The two-nucleon spectroscopic amplitudes were obtained within the shell model framework and used for the elastic transfer channel. Authors could explain the experimental data of excess cross sections by means of the CRC calculations combining both elastic scattering and elastic transfer mechanisms. Consequently, this draws attention to that the nucleus ^9Be may have also a cluster structure like $^7\text{Be} + 2n$.

In the study [13] the nuclear reactions resulting from $^3\text{He} + ^9\text{Be}$ at the energy of 63 MeV have been analyzed. The elastic channel as well as the exit channels $^7\text{Be} + ^5\text{He}$, $^6\text{Li} + ^6\text{Li}$ were calculated within the Coupled Reaction Channels (CRC) method. For these channels, all the possible transfer mechanisms were supposed. In particular, the two-step transfer mechanisms beginning with n pick-up well enhances the underestimated cross sections for the channels $^7\text{Be} + ^5\text{He}$ and $^6\text{Li} + ^6\text{Li}$. It shows that the p -shell neutron is loosely bound, and, in turn, the nucleus ^9Be has the cluster structure $^8\text{Be} + n$.

The same experimental study with the nuclear reaction $^3\text{He} + ^9\text{Be}$ was performed, but at the laboratory energy 30 MeV [14]. Pure optical model and DWBA calculations performed in this work require more sophisticated theoretical models. Therefore, our aim is to analyze the experimental data [14] within the cluster model of ^9Be and to probe all possible transfer mechanisms. We focus on the internal structure of ^9Be presenting fresh data missing in Ref. [14, 15], and on the data in more accurate processed form.

Current work is organized as follows. Detailed information of the experimental method are given in the first section. Second section is dedicated for the elastic scattering together with inelastic channel. The next section is for the cluster transfer channels. Main findings with conclusion are drawn in the end.

1. Experimental procedure

The experiment on the nuclear reaction ^3He and ^9Be at the laboratory energy of 30 MeV was conducted at the Nuclear Physics Institute (NPI), Řež, Czech Republic. In the course of the experiment time, an average beam current was kept to 10 enA. The self-supporting ^9Be target having the thickness of 11 μm was developed with the foil highly purified up to 99%. The resonances of the contamination by the carbon and oxygen isotopes were not detected in the energy spectra.

Particle identification was based on the ΔE - E method, i.e. measurements of the energy-loss ΔE and the residual energy E_r . Four Si-Si(Li) telescopes consisting of the detectors ΔE_0 , ΔE , and E_r were mounted to register scattered ions with the thicknesses of 10 μm , 100 μm , and 3 mm, respectively. The

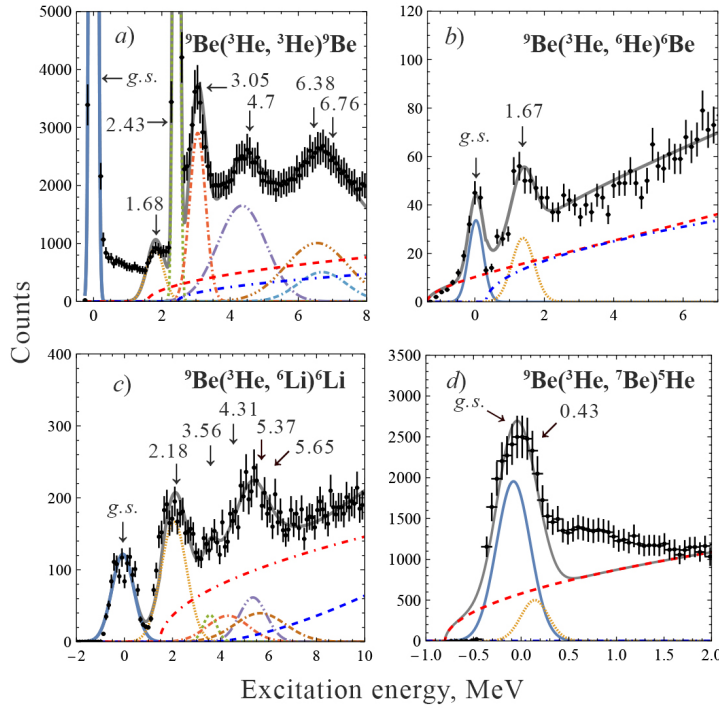


Figure 1. Excitation energy spectra of ^9Be (a), ^6Be (b), ^6Li (c) and ^5He (d) for the nuclear reaction $^3\text{He} + ^9\text{Be}$ at $E_{\text{lab}} = 30$ MeV measured at $\theta_{\text{lab}} = 12^\circ$. The total fit for each spectrum and subtracted peaks are shown. The background was fitted taking into account the three-body and four-body breakup processes (For more, please, see the text).

acceptance angle of each telescope was $\sim 0.6^\circ$ in the scattering plane, and their solid angle was ~ 0.2 msr. The good energy resolutions of both ΔE and E_r detectors provided unambiguous identification of A and Z of each product. The over-all energy resolution was 150 – 200 keV.

The excitation energy spectra for ^9Be , ^6Be , ^6Li and ^5He are shown in Fig.1. The ground and excited states of the nuclei ^9Be , ^6Be , ^6Li and ^5He were identified in the following reaction channels: $^9\text{Be} (^3\text{He}, ^3\text{He})^9\text{Be}$ (see panel a), $^9\text{Be} (^3\text{He}, ^6\text{He})^6\text{Be}$ (b), $^9\text{Be} (^3\text{He}, ^6\text{Li})^6\text{Li}$ (c) and $^9\text{Be} (^3\text{He}, ^7\text{Be})^5\text{He}$ (d). The energy calibration of the ΔE_s and E_r detectors has been performed taking into account well-known states which are strongly excited in the spectra. The calibration appeared to be practically linear. This allows us to determine the positions of all excited states in the spectra. Total energies were calculated as the sum over the calibrated energy losses ΔE_s and the residual energy E_r . The excitation energy spectra were constructed as $E_{g.s.}(\text{position}) - E_{\text{total}}$.

The peaks identified by means of the fitting procedure adopting the method of standard Gaussian decomposition. With the known energy of calibration, the positions of peaks and widths were fixed in accordance with the generally accepted experimental data. It should be noted that the width of the state in each spectrum can include: the natural width, the apparatus width of set-up and the energy spread. The latter case is originated by the emitting particles, which their production can occur either at the beginning or at the end of the target foil. The background areas are also illustrated in Fig.1. They are mainly due to the phase volumes which depend on the threshold energy in the following break-up processes:

- $^9\text{Be} \rightarrow ^8\text{Be} + n$ (see Fig. 1, panel a, red dashed curve) or $^4\text{He} + ^5\text{He}$ (a, blue dot-dashed);
- $^6\text{Be} \rightarrow ^4\text{He} + 2p$ (b, red dashed) or $^5\text{Li} + p$ (b, blue dot-dashed);
- $^6\text{Li} \rightarrow ^4\text{He} + d$ (c, red dot-dashed) or $^4\text{He} + p + n$ (c, blue dashed);

- $^5\text{He} \rightarrow ^4\text{He} + n$ (*d*, red dashed).

The absolute error in the determination of cross section is not more than 15%. Consequently, the following components can mostly contribute to the error: in the decomposition, statistical error of the number of events in the subtracted peak, error in determining the thickness of target and in the values of solid angle, loss-events, current measurement error.

2. Elastic and inelastic channels

Elastic scattering

The differential cross section of the elastic scattering of ^3He from the nucleus ^9Be was treated within the optical model framework. Numerical calculations were carried out by means of the FRESKO code [16]. The optical potential used in the OM calculations was taken in the form:

$$U(R) = -V(R) - iW(R) + V^{SO}(R)(\mathbf{1} \cdot \boldsymbol{\sigma}) + V^C(R), \quad (1)$$

where R is the distance between the ^3He and ^9Be , and V^V, W^V are the real and imaginary volume potential terms, V^{SO} and V^C are the spin-orbit and Coulomb potentials. The volume potentials may represent the Woods-Saxon (WS) potential [17]:

$$V(R) = V_0^V f_{R_V, a_V}(R), \quad f_{R_0, a_0}(R) = \left[1 + \exp\left(\frac{R - R_0}{a_0}\right) \right]^{-1}, \quad (2)$$

where V_0 is the depth of the potential, r_0 is the average distance, and a_0 is the diffusion parameter. The spin-orbit term can have the form as follows:

$$V^{SO}(R) = V_0^{SO} \left(\frac{\hbar}{m_\pi c} \right)^2 \frac{1}{R} \frac{d}{dR} f_{R_{SO}, a_{SO}}(R), \quad (3)$$

while the Coulomb term was taken as the interaction of a point-charge with a uniformly charged sphere

$$V^C(R) = \begin{cases} \frac{Z_1 Z_2 e^2}{2R_C} \left(3 - \frac{R^2}{R_C^2} \right), & \text{for } R \leq R_C, \\ \frac{Z_1 Z_2 e^2}{R}, & \text{for } R > R_C. \end{cases} \quad (4)$$

As a starting point for the seeking optical potential, we have taken global optical parameters from Ref. [18]. The elastic scattering cross section was fitted on the measured experimental data. It was performed by means of the SFRESKO [16]. Obtained potential parameters are listed in Tab. 1.

Table 1. Potential parameters used in the optical model and CRC calculations.

	V_0 , MeV	$r_V^{a)}$, fm	a_V , fm	W_0 , MeV	$r_W^{a)}$, fm	a_W , fm	V_i , MeV	$r_i^{a)}$, fm	a_i , fm	$r_C^{a)}$, fm
$^3\text{He} + ^9\text{Be}$	101.9 103.9 ^{b)}	0.700	0.777	30.81 23.81 ^{b)}	0.854	0.817	2.5 ^{c)}	0.708	0.720	0.767
$^7\text{Be} + ^5\text{He}$	258.516	0.588	0.726	18.0	0.773	0.6	45.4 ^{d)}	0.566	0.843	0.734
$^6\text{Li} + ^6\text{Li}$	114.0	0.64	0.859	45.6	0.831	0.807				0.649
$^7\text{Li} + ^5\text{Li}$	114.0	0.606	0.853	38.448	0.82	0.809				0.588
$\alpha + ^8\text{Be}$	121.0	0.252	1.01	17.0	1.38	0.34				0.724

^{a)} $r_i = R_i(A_p^{1/3} + A_t^{1/3})^{-1}$

^{b)} modified optical potential (*mOP*) used in the CRC calculations.

^{c)} i is for *SO*

^{d)} i is for imaginary first derivative of volume potential

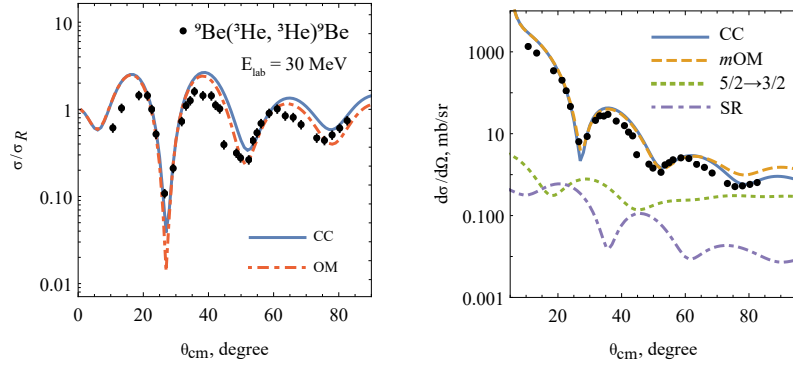


Figure 2. Theoretical cross sections for the elastic scattering $^9\text{Be}(^3\text{He}, ^3\text{He})^9\text{Be}$ in comparison with measured cross section data at $E_{lab} = 30$ MeV. Left panel: Calculated cross sections are given in ratio to the Rutherford scattering and carried out within the coupled channels (CC, $\chi^2 = 28.3$) and optical model (OM, $\chi^2 = 14.85$) methods. Right panel: the same CC cross section in absolute unit, but presented in terms of the optical model cross section with modified potential parameters (mOM), the contribution of inelastic channel ($5/2 \rightarrow 3/2$) and the spin re-orientation effect (SR).

Since the spin reorientation is not forbidden, e.g. $3/2 \rightarrow 3/2$ or $5/2 \rightarrow 5/2$, it was also taken into account in the CC calculations. The calculated CC results are presented in Fig. 2. The OM and CC calculations are almost identical. Explicit taking into account the coupling between inelastic channel and the coupling for spin reorientation modified optical potential. The real part of the optical potential becomes deeper, while the depth of the imaginary part shortens (see mOP, Tab. 1).

The role of the inelastic channel, $5/2 \rightarrow 3/2$, in the elastic channel is turned out to be non-negligible. The effect of spin reorientation stands one magnitude lower than the OM estimation. The extrema point of SR coincides with the extrema of mOP. This is one of the regular character of spin reorientation effects. Similar behaviour was also reported in Ref. [13].

Inelastic scattering

The differential cross sections for the inelastic scattering of ^3He on ^9Be with the excitation 2.43 MeV is calculated in the framework of Coupled channels (CC) method [16]. For the CC calculations, the mOP potential was used.

For the purpose of the explicit tracking of the couplings, we have not used a rotational model, but utilised the general case. In this case, the strength of the coupling factor is given by:

$$RDEF(\lambda, J \rightarrow J') = (-1)^{J+J'+|J-J'|} \sqrt{2J+1} \langle JK\lambda 0 | J'K \rangle \delta_\lambda^{J \rightarrow J'} \quad (5)$$

where J and J' are the spins of initial and final states, K is the projection. The deformation length may have the form:

$$\delta_\lambda^{J \rightarrow J'} = \beta_\lambda^{J \rightarrow J'} R_i. \quad (6)$$

Here, $\beta_\lambda^{J \rightarrow J'}$ is the deformation parameters, R_i is the interaction radius.

The calculated differential cross sections for the inelastic scattering channel with ^9Be excitation at 2.43 MeV are shown in Fig. 3. The spin re-orientation, i.e. the transition $\frac{5}{2} \rightarrow \frac{5}{2}$, has also been implemented in the coupling scheme.

The cross section of the excitation process underestimates the experimental data. However, the spin re-orientation effect enhances the cross section. Taken together, both processes are in good agreement with the experimental data. The cross section in the range starting from 65 degree is in exception, probably, due to the contributions of other excitation modes that were not included explicitly in the CC calculation.

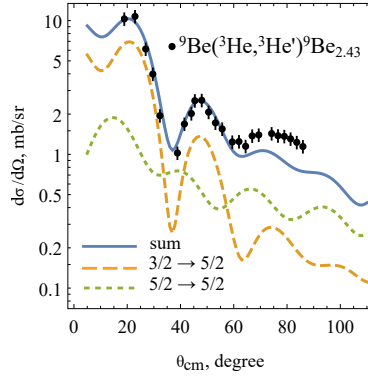


Figure 3. Inelastic scattering data in comparison with the CC calculation results in terms of different coupling contributions: the transition from $\frac{3}{2}^-$ to $\frac{5}{2}^-$ states (dashed), and spin re-orientation for the state $\frac{5}{2}^-$ (dotted).

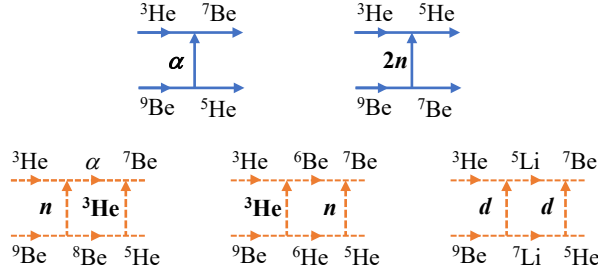


Figure 4. Reaction schemes for transfer mechanisms in $^9\text{Be} (^3\text{He}, ^7\text{Be})^5\text{He}$: one-step (solid) and two-step (dashed) mechanisms.

In this study, the best agreement of theoretical analyses with data is obtained if one uses the deformation length $\delta_2^{3/2 \rightarrow 5/2} = 1.97$ fm. The study dedicated to the scattering of α -particles on ^9Be from Ref. [19] report that the length is 1.61 fm, on the contrary the deformation length is 2.63 fm obtained in Ref. [20] in the reactions $p + ^9\text{Be}$. Our taken result on the deformation length have the middle of the values in comparing with the presented other sources. In general, the structure of ^9Be shouldn't depend on the dynamics of nuclear reactions. Nevertheless, it can be explained by the different character of interactions of the projectiles with protons and neutrons in the target nucleus [21]. Therefore, the deformation lengths deduced directly from the inelastic scattering induced by different projectiles also might be various.

In terms of the Eq.(6) the values of deformation parameters differs, since the interaction radius is ambiguous. If taken the radius parameter of the optical potential mOP $r = 0.7$ fm, the deformation parameter has 0.8, which reproduces the previous study in Ref. [22] with the same experimental data and applied theoretical method.

3. Cluster-transfer reactions

3.1. $^7\text{Be} + ^5\text{He}$ channel

In this work the reaction $^9\text{Be} (^3\text{He}, ^7\text{Be})^5\text{He}$ is supposed to have both one-step and two-step transfer mechanisms which are demonstrated schematically in Fig. 4. The one-step mechanism occurs via transferring α -particles, while the two-step mechanisms may have n - ^3He , ^3He - n , d - d . Moreover, we find that the transfer of $2n$ cluster is also possible at the backward angles of scattering. Therefore, the

CRC calculation covers all mentioned transfer mechanisms, and the resulting differential cross section for the reaction $^9\text{Be} (^3\text{He}, ^7\text{Be})^5\text{He}$ is represented as

$$\frac{d\sigma(\theta)}{d\Omega} = \frac{1}{(2J_a + 1)(2J_A + 1)} |f_I(\theta) + f_{II}(\theta)|^2, \quad (7)$$

where the amplitudes of the one-step $f_I(\theta)$ and two-step $f_{II}(\theta)$ transfer mechanisms are given as follows

$$\begin{aligned} f_I(\theta) &= f_\alpha(\theta) + f_{2n}(\theta - \pi), \\ f_{II}(\theta) &= f_{n-^3\text{He}}(\theta) + f_{^3\text{He}-n}(\theta) + f_{d-d}(\theta). \end{aligned} \quad (8)$$

The optical potential mOP is chosen as the potential for the entrance channel. For the exit channels, we have utilized an optical potential with the global optical parameters from Ref. [23].

The optical potential of the intermediate channel $\alpha + ^8\text{Be}$ has been preferred to a potential, which reproduces the experimental cross sections of $^9\text{Be} (^3\text{He}, \alpha)^8\text{Be}$ in the exit channel. The bound state wave functions have been built on the Woods-Saxon shaped potential, with the depths fitted on the binding energies. However, the resonance states were taken as the quasi-bound states, i.e. taken by means of the same procedure, but with the binding energy of 0.01 MeV. Spectroscopic amplitudes were taken from Refs. [12, 13, 24], and presented in Tab. 2.

All CRC calculations have been performed by means of the FRESKO code [16]. The two-step transfer reactions have been calculated by means of the N -step DWBA iteration neglecting the back couplings. The prior and post modes were used respectively for the first and second couplings, aimed at the avoiding the non-orthogonality term. The results of the CRC calculations are shown in Fig. 5. The optical potentials used in these calculations are given in Tab. 1.

The direct transfer of α -particle obviously prevails on other transfer mechanisms (see Fig. 5, *left panel*). It is interesting to note the different contribution of the transfer of the system $n + ^3\text{He}$. It is turned out that the system $n + ^3\text{He}$ easily transferred in the way of $n-^3\text{He}$ rather than $^3\text{He}-n$. The reason of this may lie in the p -shell valence neutron, that loosely bound to ^9Be . Next contributor to the cross section is $2n$ transfer at the backward scattering angles. Starting from 60° it gives up only α -transfer. However, starting from 90° the transfer mechanism $2n$ may stand as a main contributor. To confirm this hypothesis, one must carry out the experiment at energies much higher than the energy in the present work, i.e. 30 MeV. Thus, it would come to possible in the identifying of registered particles at the back hemisphere. In similar experimental studies [12, 13] the $2n$ cluster transfer from ^9Be was also explored. In particular, the transfer of $2n$ cluster was observed by Umbelino *et al* [12] in the elastic

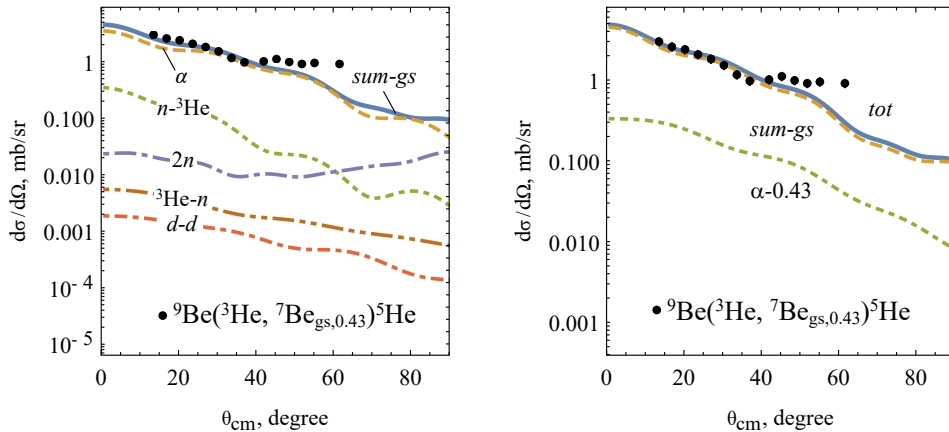


Figure 5. Calculated CRC cross sections with the experimental data for the nuclear reaction $^9\text{Be} (^3\text{He}, ^7\text{Be}_{\text{gs},0.43})^5\text{He}$. Cross sections are shown in terms of each considered transfer mechanisms to the ground state of ^7Be (left panel). Incoherent sum of cross sections over the ground and first excited 0.43 states of ^7Be (right panel).

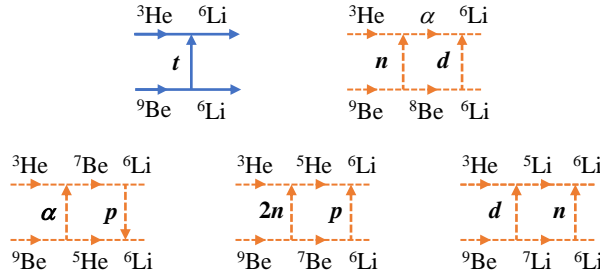


Figure 6. Same as the caption of Fig. 4 but for the reaction $^9\text{Be}(^3\text{He}, ^6\text{Li})^6\text{Li}$.

transfer reactions $^7\text{Be} + ^9\text{Be}$. The transfer mechanism $d-d$ has the lowest contribution among all of the proposed transfer mechanisms.

As a consequence of low detector resolution, we couldn't differ the registered ^7Be at the ground and first excited states. Nevertheless, we could have estimated its weight to the cross section via CRC calculations. It turned out the cross section to the first excited state impacts less notably than the transfer mechanism n - ^3He (see Fig. 5, *right panel*). The calculated CRC cross sections reproduce experimental data well, except last few points, that have not been described with the proposed model.

3.2. $^6\text{Li} + ^6\text{Li}$ channel

The transfer mechanisms of the cluster t is suggested to have also two-step processes as well, as it was suggested in Ref. [13]. The direct transfer t , and two-step transfer mechanisms of the cluster t (see Fig. 6): n - d , α - p , $2n$ - p , and d - n , were included in the CRC calculations. Differential cross sections for these transfer mechanisms are obtained analogously as in Eq. 7.

CRC calculations for the transfer of the cluster t have included the optical potential WS as for the entrance channel, and a Woods-Saxon shaped potential for the exit channel $^6\text{Li} + ^6\text{Li}$. The potential parameters of the exit channel was extracted by fitting the experimental data on the elastic scattering $^6\text{Li} + ^6\text{Li}$ at the energy 40 MeV [25]. Obtained optical potential is shown in Tab. 1.

Apart from the fact that ^6Li was detected at the ground state, there were also two registered resonances. In the CRC calculations, they were taken into account through the coupling with the

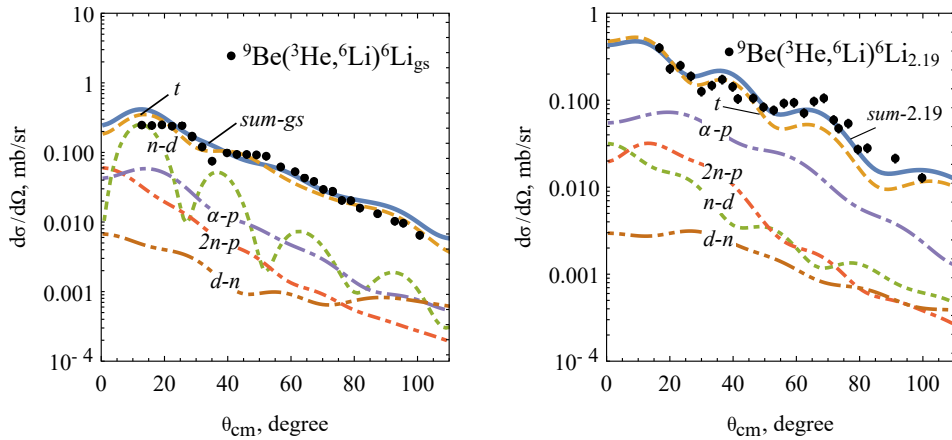


Figure 7. Experimental data for nuclear reaction $^9\text{Be}(^3\text{He}, ^6\text{Li})^6\text{Li}_{\text{gs}}$ (left panel) and $^9\text{Be}(^3\text{He}, ^6\text{Li})^6\text{Li}_{2,19}$ (right panel) compared to the calculated CRC cross sections in terms of channel contributions (For more, please, see the text).

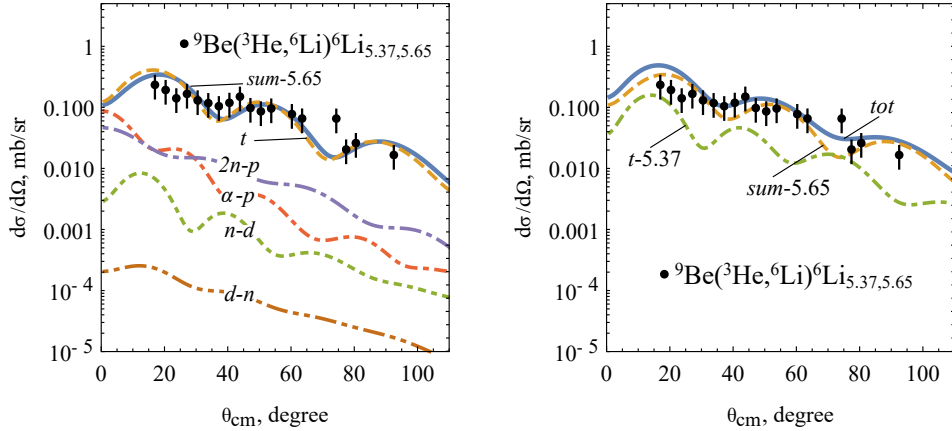


Figure 8. Experimental data for nuclear reaction $^9\text{Be} (^3\text{He}, ^6\text{Li}) ^6\text{Li}_{5,37,5.65}$ compared to the CRC calculation results. The CRC cross section for the target-like nucleus $^6\text{Li}^*$ at 5.65 MeV with the channel contributions (left panel). Total cross section summed incoherently over 5.65 MeV and 5.37 MeV channels (right panel).

ground state of ^6Li .

The calculated differential cross sections for the channel $^6\text{Li} + ^6\text{Li}$ at the ground state are presented in Fig. 7 (*left panel*) with the contributions of each transfer mechanisms. The direct transfer of the cluster t dominates at the whole range of angles. The two-step transfer mechanism $n-d$ is turned out to be less contributor than the transfer mechanism t in contrary to the studies by Rudchik *et al* [13] within the same reaction, but at the laboratory energy of 63 MeV. In the work the role of the transfer mechanism $n-d$ prevails over other processes including the direct transfer t . The cross section of the mechanism $n-d$ has an oscillatory character, and competes with the mechanism $\alpha-p$. The latter transfer mechanisms, i.e. $2n-p$ and $d-n$, are insignificantly involved to the reaction.

Contribution order changes, when ^6Li gets excited (see Fig. 7, *right panel*). The transfer mechanism t remains unchanged, while $\alpha-p$ stands as the next contributor. Weakening of the mechanism $n-d$ can be interpreted as the switching value in the spectroscopic amplitudes. In particular, the amplitude for the overlap $(^6\text{Li}_{2,19} | ^8\text{Be})$ with the configuration $2S_1$ is changed to 0.089. Such the small spectroscopic amplitude must have brought $n-d$ far below than the transfer mechanism $d-n$. However, the spectroscopic amplitudes with $1D_{1,2,3}$ have non-negligible values: 0.414, -0.477 , and 0.744, that do not allow $n-d$ to disappear in the reaction.

Two resonances at 5.37 MeV and 5.65 MeV are mixed in the differential cross sections due to the experimental limitations. Therefore, we have included two channels into the CRC calculations. Calculation results for $^9\text{Be} (^3\text{He}, ^6\text{Li}) ^6\text{Li}^*$ with the excitation 5.65 MeV are demonstrated in Fig. 8 (*left panel*) in comparing with experimental data. The reaction mainly occurs through the direct transfer of cluster t . Two transfer mechanisms, $2n-p$ and $\alpha-p$, affect nuclear reaction only up to 30° . Other transfer mechanisms, i.e. $n-d$ and $d-n$, almost do not influence the reaction.

Due to the fact that the transfer of cluster t has been the leading contributor in the $^6\text{Li} + ^6\text{Li}$ channel, the channel with the excitation 5.37 MeV calculated only with the transfer of t . The differential cross section of the channel of the 5.37 MeV excited state added incoherently with the channel at 5.65 MeV. Total cross section resulting from the CRC calculations are shown in Fig.8 (*right panel*). The channel $^6\text{Li} + ^6\text{Li}^*$ with the excitation 5.37 MeV has got less contribution than the channel at 5.65 MeV. Calculated differential cross sections reproduces experimental data well.

Table 2. Spectroscopic information data used in the CRC calculations for Composite (A) consisted of Core (C) and Valence particle (ν) with configuration nlj . Most of Spectroscopic amplitudes (SA) were taken from Refs. [12,13,24]

A	C	ν	nlj	SA	A	C	ν	nlj	SA				
^6Li	1	^3He	0.5 t	0.5	$2S_{0.5}$	-0.943	^9Be	1.5	^5He	1.5 α	0	$2D_2$	-0.530
^6Li	3	^3He	0.5 t	0.5	$1D_{2.5}$	-0.943	^7Be	1.5	^6Li	1_1 p	0.5	$1P_{0.5}$	-0.657
^6Li	1	^3He	0.5 t	0.5	$1D_{1.5}$	0.943	^7Be	1.5	^6Li	3 p	0.5	$1P_{1.5}$	0.738
^9Be	1.5	^6Li	1_1 t	0.5	$2P_{0.5}$	-0.192	^7Be	1.5	^6Li	1_2 p	0.5	$1P_{0.5}$	0.147
^9Be	1.5	^6Li	1_1 t	0.5	$2P_{1.5}$	-0.215	^7Be	1.5	^6Li	1_2 p	0.5	$1P_{1.5}$	-0.132
^9Be	1.5	^6Li	3 t	0.5	$2P_{1.5}$	-0.594	^7Be	1.5	^6Li	1_1 p	0.5	$1P_{1.5}$	-0.735
^9Be	1.5	^6Li	3 t	0.5	$1F_{3.5}$	-0.316	^6Li	1_1	^5He	1.5 p	0.5	$1P_{0.5}$	-0.596
^9Be	1.5	^6Li	1_2 t	0.5	$2P_{0.5}$	-0.118	^6Li	1_1	^5He	1.5 p	0.5	$1P_{1.5}$	0.667
^9Be	1.5	^6Li	1_2 t	0.5	$1F_{2.5}$	-0.324	^6Li	3	^5He	1.5 p	0.5	$1P_{1.5}$	0.500
^4He	0	^3He	0.5 n	0.5	$1S_{0.5}$	-0.741	^6Li	1_2	^5He	1.5 p	0.5	$1P_{0.5}$	0.333
^9Be	1.5	^8Be	0 n	0.5	$1P_{1.5}$	0.791	^6Li	1_2	^5He	1.5 p	0.5	$1P_{1.5}$	0.298
^9Be	2.5	^8Be	0 n	0.5	$1P_{1.5}$	-0.816	^5Li	1.5	^3He	0.5 d	1	$1P_1$	0.456
^9Be	2.5	^8Be	2 n	0.5	$1P_{1.5}$	-0.986	^5Li	1.5	^3He	0.5 d	1	$1P_2$	1.021
^9Be	2.5	^8Be	0 n	0.5	$1P_{0.5}$	0.242	^9Be	1.5	^7Li	1.5 d	1	$2S_1$	-0.226
^9Be	2.5	^8Be	2 n	0.5	$1P_{0.5}$	0.417	^9Be	1.5	^7Li	1.5 d	1	$1D_1$	0.111
^6Li	1.0	^4He	0 d	1.0	$2S_1$	1.061	^9Be	1.5	^7Li	1.5 d	1	$1D_3$	-0.624
^6Li	3.0	^4He	0 d	1.0	$1D_3$	1.061	^6Li	1_1	^5Li	1.5 n	0.5	$1P_{0.5}$	0.597
^8Be	0	^6Li	1_1 d	1.0	$2S_1$	1.146	^6Li	1_1	^5Li	1.5 n	0.5	$1P_{1.5}$	-0.667
^8Be	0	^6Li	1_1 d	1.0	$1D_1$	0.112	^6Li	3	^5Li	1.5 n	0.5	$1P_{1.5}$	1.095
^8Be	0	^6Li	3 d	1.0	$2S_1$	0.089	^6Li	1_2	^5Li	1.5 n	0.5	$1P_{0.5}$	-0.333
^8Be	0	^6Li	3 d	1.0	$1D_1$	0.414	^6Li	1_2	^5Li	1.5 n	0.5	$1P_{1.5}$	-0.298
^8Be	0	^6Li	3 d	1.0	$1D_2$	-0.477	^7Li	1.5	^6Li	1_1 n	0.5	$1P_{0.5}$	-0.657
^8Be	0	^6Li	3 d	1.0	$1D_3$	0.744	^7Li	1.5	^6Li	1_1 n	0.5	$1P_{1.5}$	-0.735
^8Be	0	^6Li	3 d	1.0	$2S_1$	0.850	^7Li	1.5	^6Li	3 n	0.5	$1P_{1.5}$	0.738
^8Be	2	^6Li	3 d	1.0	$2S_1$	0.747	^7Li	1.5	^6Li	1_2 n	0.5	$1P_{0.5}$	0.147
^8Be	2	^6Li	3 d	1.0	$1D_1$	0.079	^7Li	1.5	^6Li	1_2 n	0.5	$1P_{1.5}$	-0.132
^8Be	2	^6Li	3 d	1.0	$1D_2$	0.259	^6He	0	^5He	1.5 n	0.5	$1P_{1.5}$	-0.867
^8Be	2	^6Li	3 d	1.0	$1D_3$	0.538	^7Be	1.5	^6Be	0 n	0.5	$1P_{1.5}$	-0.935
^8Be	0	^6Li	1_2 d	1.0	$2S_1$	-0.237	^6He	0	^4He	0 $2n$	1.0	$1S_0$	0.909
^8Be	0	^6Li	1_2 d	1.0	$1D_1$	0.372	^8Be	0	^6Be	0 d	1.0	$1S_0$	-1.200
^8Be	2	^6Li	1_2 d	1.0	$2S_1$	0.371	^7Be	1.5	^4He	0 ^3He	0.5	$2P_{1.5}$	-1.091
^8Be	2	^6Li	1_2 d	1.0	$1D_1$	0.053	^8Be	0	^5He	1.5 ^3He	0.5	$2P_{1.5}$	-1.102
^8Be	2	^6Li	1_2 d	1.0	$1D_2$	-0.356	^6Be	0	^3He	0.5 ^3He	0.5	$2S_{0.5}$	0.943
^8Be	2	^6Li	1_2 d	1.0	$1D_3$	-0.130	^9Be	1.5	^6He	0 ^3He	0.5	$2P_{1.5}$	-0.215
^5He	1.5	^3He	0.5 $2n$	0	$1P_1$	-0.913	^7Be	1.5	^6Be	0 n	0.5	$1P_{0.5}$	-1.091
^9Be	1.5	^7Be	1.5 $2n$	0	$2S_0$	0.247	^6He	0	^5He	1.5 n	0.5	$1P_{1.5}$	-1.102
^9Be	1.5	^7Be	1.5 $2n$	0	$2D_2$	0.430	^7Be	1.5	^5Li	1.5 d	1	$2S_1$	-0.647
^6Li	1_1	^5He	1.5 p	0.5	$1P_{0.5}$	-0.597	^7Be	1.5	^5Li	1.5 d	1	$1D_1$	-0.121
^6Li	1_1	^5He	1.5 p	0.5	$1P_{1.5}$	0.667	^7Be	1.5	^5Li	1.5 d	1	$1D_3$	0.647
^7Be	1.5	^6Li	1_1 p	0.5	$1P_{0.5}$	-0.657	^7Li	1.5	^5He	1.5 d	1	$1D_3$	0.647
^7Be	1.5	^6Li	1_1 p	0.5	$1P_{1.5}$	-0.735	^7Li	1.5	^5He	1.5 d	1	$2S_1$	-0.647
^7Be	1.5	^6Li	2 p	0.5	$1P_{1.5}$	-1.095	^7Li	1.5	^5He	1.5 d	1	$1D_1$	-0.121
^7Be	1.5	^6Li	1_2 p	0.5	$1P_{1.5}$	-0.632	^7Li	1.5	^5He	1.5 d	1	$1D_3$	0.647
^7Be	1.5	^6Li	1_2 p	0.5	$1P_{0.5}$	-0.632	^7Be	1.5	^3He	0.5 α	0	$2P_1$	-0.950
^7Be	1.5	^3He	0.5 α	0	$2P_1$	1.091	^9Be	1.5	^5He	1.5 α	0	$3S_0$	-0.810
^9Be	1.5	^5He	1.5 α	0	$3S_0$	-0.810	^9Be	1.5	^5He	1.5 α	0	$2D_2$	-0.536

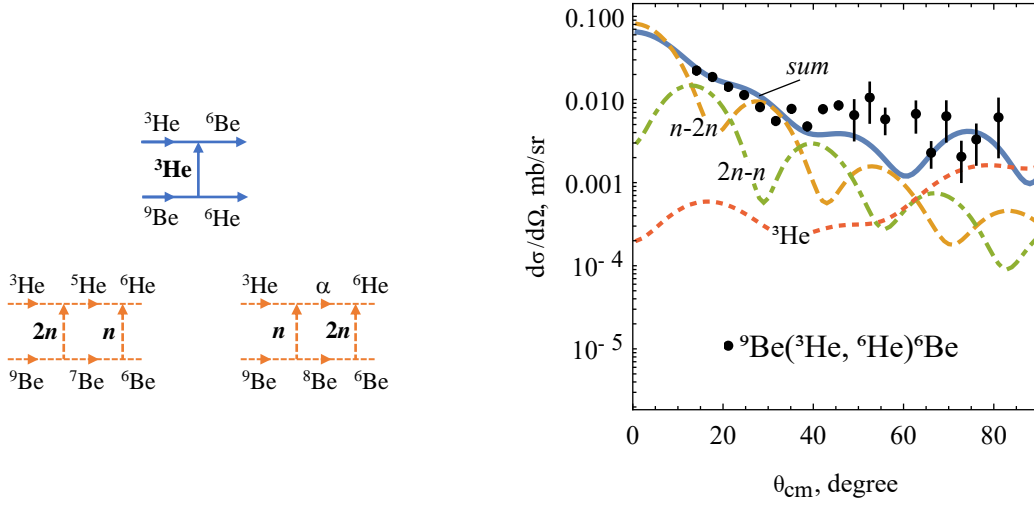


Figure 9. Left panel: reaction schemes for one- (solid) and two-step (dashed) transfer mechanisms for $^9\text{Be}(^3\text{He}, ^6\text{He})^6\text{Be}$. Right panel: comparison of the CRC differential cross sections with the experimental data for the same reaction.

3.3. $^6\text{He} + ^6\text{Be}$ channel

The channel $^6\text{He} + ^6\text{Be}$ is a unique channel, since the transfer of the system $3n$ is observed at the forward angles of scattering. In this case, here we suggest three mechanisms of transfer (see Fig. 9, *left panel*): the two-step $n-2n$ and $2n-n$, and the one-step transfer of the cluster ^3He at the back hemisphere. Differential cross sections are obtained as well as they are expressed in Eq. 7. The resulting CRC calculations on cross sections in terms of each contribution followed three mechanisms are demonstrated in Fig. 9, (*right panel*).

The two-step transfer mechanisms, i.e. $n-2n$ and $2n-n$, compete with each other to give almost smooth cross section. Starting from 60° the most contribution is caused by the transfer of ^3He . Calculated CRC calculations are in good agreement with the experimental data.

However the CRC calculations for the channel $^6\text{He} + ^6\text{Be}$ have been performed using the large valued spectroscopic amplitudes. For example, the overlaps $\langle ^6\text{He} | \alpha \rangle$, $\langle ^6\text{Be} | ^8\text{Be} \rangle$ have the amplitudes ~ 1.2 . On the contrary the studies [26, 27] reported the amplitude for $\langle ^6\text{He} | \alpha \rangle$ equals ~ 1.0 . Such kind of difference between spectroscopic amplitudes points out that there may have other processes not included in the reaction model. Probably, the one-step transfer of the system $3n$ can take place in the channel $^6\text{He} + ^6\text{Be}$. This problem is a separate topic of study, and it cannot precisely solved by the model shown in this work. For more accurate results one might apply using the four body problem.

Conclusion

The nuclear reactions with ^9Be induced with the ^3He at 30 MeV was investigated. Elastic channel treated within the optical model, while inelastic channel was considered by means of the Coupled channels approach. New parameters of the optical potential for the system $^3\text{He} + ^9\text{Be}$ at 30 MeV were obtained. Using the optical potential the deformation parameter $\delta_2^{3/2 \rightarrow 5/2} = 0.8$ was extracted within the CC method, which could reproduce the results from another source [22].

All possible transfer mechanisms were suggested in the cluster transfer channels, $^7\text{Be} + ^5\text{He}$, $^6\text{Li} + ^6\text{Li}$, and $^6\text{He} + ^6\text{Be}$. Differential cross sections for these transfer mechanisms were calculated in the CRC framework using the Spectroscopic amplitudes and optical potentials without any corrections. The primary pick-up of valence neutron turned out to be easily picked-up in the cluster transfer channels, except in the channels with the ^6Li excitations. This manner specifies the cluster structure $n + ^8\text{Be}$ in ^9Be .

Special attention attracts the channel $^6\text{He} + ^6\text{Be}$. In the CRC framework, we could obtain good agreement of the calculated cross sections with data suggesting the two-step transfer mechanisms, n - $2n$ and $2n$ - n . However, the large valued spectroscopic amplitudes used in the CRC point out that there may play other processes, e.g. direct transfer of three neutrons.

The one-nucleon transfer channels, as well as the charge exchange reaction channels, are planned to investigate as a continued of the series of studies dedicated to the reaction $^3\text{He} + ^9\text{Be}$ at the energy of 30 MeV.

Acknowledgements

We would like to thank the NPI (Nuclear Physics Institute) Řež for giving us the opportunity to perform this study, as well as the cyclotron staff of institutes for the excellent beam quality.

This research was funded by the Science Committee of the Ministry of Science and Higher Education of the Republic of Kazakhstan (Grant No. AP14870958).

References

- [1] Karpov A, Denikin A, Naumenko M, Alekseev A, Rachkov V, Samarin V, Saiko V and Zagrebaev V 2017 *Nuclear Instruments and Methods in Physics Research Section A: Accelerators, Spectrometers, Detectors and Associated Equipment* **859** 112 – 124
- [2] Lederer C and Shirley V 1978 *Table of Isotopes John Wiley & Sons* (7th edition John Wiley and Sons, New York, USA)
- [3] Ajzenberg-Selove F 1988 *Nuclear Physics A* **490** 1–225
- [4] Lichtenthäler R, Santos O, Serra A, Umbelino U, Pires K, Oliveira J, Lépine-Szilý A, de Faria P and Morcelle V 2021 *The European Physical Journal A* **57** 1–13
- [5] Huang B S, Ma Y G *et al.* 2021 *Physical Review C* **103** 054318
- [6] Fortune H 2021 *Nuclear Physics A* **1014** 122249
- [7] Starastin V, Demyanova A, Danilov A, Ogloblin A, Dmitriev S, Goncharov S, Lin C J, Yang L, Wang D X, Jia H M *et al.* 2021 *The European Physical Journal A* **57** 1–12
- [8] Maridi H, Pakou A and Rusek K 2021 *International Journal of Modern Physics E* **30** 2150024
- [9] Mahmoud Z M and Qandil O S 2021 *Physics of Atomic Nuclei* **84** 711–723
- [10] Amar A 2022 *International Journal of Modern Physics E* **31** 2250011
- [11] Amar A and Ibraheem A A 2021 *International Journal of Modern Physics E* **30** 2150090–172
- [12] Umbelino U, Pires K, Lichtenthäler R, Scarduelli V, Scotton G, Lépine-Szilý A, Guimaraes V, Lubian J, Paes B, Ferreira J *et al.* 2019 *Physical Review C* **99** 064617
- [13] Rudchik A, Koshchy E, Budzanowski A, Siudak R, Szczurek A, Skwirczyńska I, Mashkarov Y G, Głowacka L, Turkiewicz J, Zalyubovsky I *et al.* 1996 *Nuclear Physics A* **609** 147–162
- [14] Lukyanov S, Harakeh M, Naumenko M, Xu Y, Trzaska W, Burjan V, Kroha V, Mrazek J, Glagolev V, Piskoř Š *et al.* 2016 Cluster structure of ^9Be from $^3\text{He} + ^9\text{Be}$ reaction *Journal of Physics: Conference Series* vol 724 (IOP Publishing) p 012031
- [15] Urazbekov B 2023 Three-nucleon transfer mechanisms in the reaction induced by 30 mev ^3He on ^9Be *Journal of Physics: Conference Series* vol 2453 (IOP Publishing) p 012015
- [16] Thompson I J 1988 *Computer Physics Reports* **7** 167–212
- [17] Woods R D and Saxon D S 1954 *Physical Review* **95** 577
- [18] Becchetti Jr F and Greenlees G 1971 *Polarization Phenomena in Nuclear Reactions (Proceedings no 3)* (University of Wisconsin Press)
- [19] Harakeh M, Van Popta J, Saha A and Siemssen R 1980 *Nuclear Physics A* **344** 15–40
- [20] Votava H, Clegg T, Ludwig E and Thompson W 1973 *Nuclear Physics A* **204** 529–551
- [21] Jiang Y, Lou J L, Ye Y L, Liu Y, Tan Z W, Liu W, Yang B, Tao L C, Ma K, Li Z H, Li Q T, Yang X F, Xu J Y, Yu H Z, Han J X, Bai S W, Huang S W, Li G, Wu H Y, Zang H L, Feng J, Chen Z Q, Chen Y D, Yuan Q, Li J G, Hu B S, Xu F R, Wang J S, Yang Y Y, Ma P, Hu Q,

- Bai Z, Gao Z H, Duan F F, Hu L Y, Tan J H, Sun S Q, Song Y S, Ong H J, Tran D T, Pang D Y and Yuan C X (RIBLL Collaboration) 2020 *Phys. Rev. C* **101**(2) 024601
- [22] Janseitov D, Lukyanov S, Mendibayev K, Penionzhkevich Y E, Skobelev N, Sobolev Y G, Kuterbekov K, Valiolda D, Zholdybayev T, Trzaska W *et al.* 2018 *International Journal of Modern Physics E* **27** 1850089
- [23] Cook J 1982 *Nuclear Physics A* **388** 153–172
- [24] Kurath D and Millener D 1975 *Nuclear Physics A* **238** 269–286
- [25] Potthast K, Brand H, Freiesleben H, Rosenthal P, Kamys B, Sydow L *et al.* 1997 *Nuclear Physics A* **614** 95–111
- [26] Oganessian Y T, Zagrebaev V and Vaagen J 1999 *Physical Review C* **60** 044605
- [27] Khoa D T and Von Oertzen W 2004 *Physics Letters B* **595** 193–201